Petroleum 4 (2018) 398–407

Contents lists available at ScienceDirect

Petroleum

journal homepage: www.keaipublishing.com/en/journals/petlm

CO_2 sequestration through direct aqueous mineral carbonation of red gypsum

Amin Azdarpour [a, *], Mohammad Afkhami Karaei [a], Hossein Hamidi [b], Erfan Mohammadian [c], Bizhan Honarvar [a]

[a] Department of Petroleum Engineering, Marvdasht Branch, Islamic Azad University, Marvdasht, Iran
[b] School of Engineering, University of Aberdeen, Aberdeen AB24 3UE, UK
[c] Faculty of Chemical Engineering, Universiti Teknologi MARA, 40450 Shah Alam, Selangor, Malaysia

ARTICLE INFO

Article history:
Received 8 October 2016
Received in revised form
9 September 2017
Accepted 18 October 2017

Keywords:
Red gypsum
Titanium dioxide
Characterization
Direct mineral carbonation
Carbon dioxide sequestration

ABSTRACT

In this study, the physical and chemical characteristics and direct aqueous mineral carbonation of red gypsum have been investigated. The characterization studies showed that red gypsum is a very potential feedstock for mineral carbonation. It is mainly consisted of CaO, Fe_2O_3 and SO_3 along with some impurities. On the other hand, the carbonation results showed that direct aqueous carbonation of red gypsum resulted in $CaCO_3$ and $FeCO_3$ production, however, the carbonates purity and carbonation efficiency are still very low.

1. Introduction

Globally, 75% of CO_2 being emitted into atmosphere are mostly contributed by the consumption of fossil fuels. At present, 86% of the world energy consumption is supplied from the fossil fuel. Over dependence on fossil fuel has resulted in an increase in the CO_2 concentration from 280 ppm in the 1750s to over 400 ppm in 2015. As a result, the global temperature has already been increased by 1 °C and is predicted to be increased by 1.8–4 °C by 2100 [1–5]. Reducing the fuel consumption by increasing the process efficiency, switching energy source to non–fossil fuels, and enhancing CO_2 sequestration by developing technologies are the available and applicable methods of reducing atmospheric CO_2 concentration [1,5–7]. The CO_2 capture efficiency of more than 80% as well as applicability to large CO_2 emission sources make carbon capture and storage strategies one of the best CO_2 reduction techniques. The contribution of up to 15–55% of the cumulative global climate change mitigation effort by 2100 has been predicted by employing the CCS methods [1,7–10].

Mineral carbon dioxide sequestration is an exothermic chemical reaction of a metal–bearing oxide, usually calcium (Ca), magnesium (Mg), or iron (Fe), with CO_2 to form stable solid carbonates. Carbonation can take place either in-situ or ex-situ. In–situ carbonation is the reaction of CO_2 with Mg and Ca minerals underground where CO_2 is being injected, and ex-situ carbonation is the same reaction taking place above ground in a chemical processing plant [11–13]. The CO_2 mineralization, or mineral carbonation, is an artificial rock weathering whereas natural rock weathering is a geological time-scale process. Mineral carbonation provides a permanent and leakage–free CO_2 disposal method in that the produced carbonates are environmentally benign and stable [14–16]. Mineral carbonation is also considered to be the best option for mineral sequestration where underground formations are not available and other sequestration methods are not feasible, such as in Finland, Korea and Lithuania. Natural minerals and industrial by-products rich in Ca and Mg can undergo the carbonation reaction through direct and indirect mineral carbonation processes [12,15,17].

* Corresponding author.
E-mail addresses: amin.azhdarpour@miau.ac.ir, aminazh22@gmail.com (A. Azdarpour).

Peer review under responsibility of Southwest Petroleum University.

Production and Hosting by Elsevier on behalf of KeAi

https://doi.org/10.1016/j.petlm.2017.10.002

Recently red gypsum has received an attention to be used as a feedstock for mineral carbonation purposes. Azdarpour et al. [18] investigated the feasibility of direct carbonation of red gypsum through Mersberg process. They investigated the effects of reaction temperature, CO_2 pressure and red gypsum particle size on products purity and carbonation efficiency. Their experiments showed that two main products including $CaCO_3$ and $FeCO_3$ can be produced by direct injection of CO_2 into red gypsum slurry. However, experiments showed that $CaCO_3$ purity and calcium carbonation efficiency were always higher than $FeCO_3$ purity and iron carbonation efficiency. They also concluded that increasing CO_2 pressure as well as particle size reduction have positive influence on increasing the overall efficiency of the carbonation process. On the other hand, carbonation efficiency first increased and then decreased with increasing reaction temperature. In another study by the Azdarpour et al. [19], the feasibility of Ca and Fe extraction from red gypsum with different mineral acids were investigated. In addition, the kinetics involved during Ca/Fe extraction from red gypsum were explored. They found that H_2SO_4 was more effective than HCl and HNO_3 in extracting Ca and Fe from red gypsum. Moreover, Ca/Fe extraction from red gypsum was kinetically controlled by the combination of product layer diffusion and chemical reaction control. They concluded that Ca/Fe can be effectively extracted from red gypsum for the purpose of indirect carbonation process.

Indirect carbonation of red gypsum was investigated by Pérez-Morene et al. [20]. They utilized two different alkaline solutions including NaOH and NH_4OH in the extraction step. Each solution was continuously stirred for 3 h at room temperature. Subsequently, the solid $Ca(OH)_2$ formed was dissolved in water with a flow of CO_2 through the suspension for 1 h, and the carbonation reaction took place at constant temperature of 75 °C. They concluded that the conversion of red gypsum to calcium carbonate was 92% when using NaOH, whereas 64% was obtained with NH_4OH extracting. In another study by Azdarpour et al. [21] the effect of CO_2 pressure on pH swing carbonation of red gypsum was explored. They concluded that carbonation efficiency was directly affected by the CO_2 pressure and the maximum efficiency (100%) was achieved when 8 bar CO_2 pressure was used. In addition, carbonation experiments resulted in $CaCO_3$ production in the form of calcite, aragonite, and vaterite with maximum purity of 98%.

Only few studies have been conducted on red gypsum carbonation and the most effective process route is yet to be identified, however, the previous studies have proven that red gypsum can be a very suitable feedstock for mineral carbonation. The previous studies have presented some of physical and chemical properties of red gypsum, however, for future deployment of red gypsum a comprehensive physico-chemical analysis of red gypsum is essential. Therefore, this study focuses the evaluation of the physical and chemical characteristics of red gypsum using X-ray diffraction (XRD), X-ray fluorescence (XRF), field emission scanning electron microscope (FESEM), thermal gravimetric analysis (TGA), fourier transform infrared spectroscopy (FT-IR), inductively coupled plasma optical emission spectrometry (ICP-OES) and particle size analyzer. Moreover, in order to have a better understanding on red gypsum carbonation, different sets of direct aqueous carbonation were conducted. The effects of CO_2 pressure, reaction temperature, particle size, and reaction time on carbonation efficiency and carbonates purity were investigated. The carbonation experimental results provide more knowledge on carbonation potential of red gypsum for future development.

2. Materials and methods

2.1. Materials

Fresh red gypsum samples used in this study were obtained from landfill of Huntsman Tioxide, Kemaman, Terengganu, Malaysia. The samples were dried in an oven overnight at 45 °C.

2.2. Characterization of red gypsum

2.2.1. Chemical analysis

The major elements and compounds of red gypsum were determined by using XRF. To minimize the error while performing the XRF, samples were made as homogenous as possible. The method explained by Gázquez et al. [22] was used, in which 1 g of red gypsum and 10 g of lithium tetraborate (a material used for melting) was prepared. Then, samples were mixed with five drops of 20% lithium iodine. To fuse the sample, the prepared mixture was placed in a crucible of Pt–Au and inserted in a furnace. Finally the produced homogenous glass sample was introduced to the XRF machine for phase determination.

FT-IR absorbance spectra were measured by a Bruker Tensor 27 spectrometer. The analysis was carried out in the mid-infrared region from 4000 cm^{-1} to 500 cm^{-1} with a resolution of 4 cm^{-1}. For each sample, 2 individual scans were recorded and averaged to obtain the spectrum. Each collected spectrum was measured in ambient air against that of pure KBr as a background spectrum. The data processing was carried out using the software OPUS 6.5, including (i) atmospheric correction for carbon dioxide (CO_2) and water, (ii) baseline correction, (iii) normalization to compensate for fluctuations in ambient conditions using the band at 1034 cm^{-1} and setting its absorbance to 2 and setting the lowest spectra absorbance value to zero, and (iv) using of the second derivative to smooth the spectrum and reduce its noise.

Trace elements have been determined by ICP-OES using an HP4500® system after the total dissolution of the samples and its posterior dilution and adaptation for their introduction in the system in 2% nitric acid. The data processing was undertaken using Plasmalab software (version 2.5.4, Thermo-Fisher Scientific, UK).

2.2.2. Mineralogical analysis

Samples of red gypsum were dried overnight in the oven and then introduced into the XRD machine. For qualification of mineral phases, 1 g of red gypsum sample was analyzed using a Philips Analytical 1050 X-ray Diffraction (XRD) at a scan speed of 1°/min from 5° to 70° under 40 kV/40 mA.

2.2.3. Physical analysis

A FESEM JEOL JSM-6400 was employed to study the morphology and composition of the particles. Secondary electron (SE) images were collected using 20 kV beam voltage and 15 mm working distance and the chemical microanalyses were performed with a Link ISIS 300 EDX microanalysis system fitted with a Si (Li) detector. FESEM analyses required 1000 mg representative finely ground samples, which were adhered to a carbon tab prior to sputter a coating with gold at 2.2 kV for 90 s.

Granulometry (particle size distribution) has been achieved by using a MASTERSIZER 2000 APA 2000 system (©Malvern Instruments Ltd.), which is based on the Mie theory, i.e., in the dispersion of the light by the grains of the material to be analyzed when these grains are in suspension in water. The dispersion pattern depends on the grain size. For a proper granulometry measurement, a representative amount of each sample was placed

in water for 24 h to achieve a high level of disintegration of the original matrix and, afterwards, introduced into a magnetic separator at a constant speed of 700 laps per min before its collection by the MASTERSIZER 2000 system for analysis.

The weight loss of red gypsum was investigated by TGA analyses performed using a thermal TGA Q500, TA Instrument. A representative red gypsum sample (20 mg) was heated in alumina cups under nitrogen atmosphere at 10 °C/min from ambient to 1000 °C. The temperature was held for 10 min at 105 °C, 650 °C and 850 °C to provide complete decomposition of bond water and also CO_2 if there was any in the red gypsum. The weight loss in the temperature region of 25–1000 °C was determined to be the decomposition of red gypsum.

2.3. Carbonation experiments

Carbonation experiments were performed in a 100 mL high pressure high temperature autoclave reactor as shown in Fig. 1. The maximum operating pressure of autoclave reactor is 200 bar, and the maximum operating temperature is about 450 °C, respectively. A batch of 10 g red gypsum with the specific average particle size and 50 mL Nanopure-demineralized water were prepared and poured into the reactor. The suspension was stirred at a specific stirring rate of 1000 rpm for about 10 min prior to CO_2 injection. The reactor was then sealed air tightly and heated to the desired reaction temperature (25–400 °C). After stabilizing the reaction temperature at the set point, CO_2 was injected into the reactor at the desired pressure (1–70 bar). The carbonation reactions were stopped after reaction time was elapsed. To keep the constant concentration of CO_2 inside the reactor, the pressure was maintained constant in the autoclave reactor using a special gas regulator having 1–70 bar outlet gas pressure. Finally, carbonation product was collected, dried overnight at 105 °C, and further analyzed using TGA and XRD.

After drying the products, some samples were analyzed with XRD for phase detection. The purity of produced carbonates was also measured using TGA results. Because red gypsum contains a significant amount of Ca and Fe, the possibility of producing both Ca carbonate ($CaCO_3$) and Fe carbonate ($FeCO_3$) was examined. In this study, $CaCO_3$ purity is defined as the percentage of $CaCO_3$ in the final product. The purity of $CaCO_3$ and $FeCO_3$ was calculated using Equations (1) and (2), respectively. In these equations, *P* stands for product purity, ΔW is the sample weight loss from TGA and MW stands for molecular weights. The weight loss of $FeCO_3$ occurs at 200–450 °C, and weight loss of $CaCO_3$ occurs at 600–850 °C due to CO_2 evaporation. The mass of Ca and Fe ions in carbonate was calculated using Equations (3) and (4), and then carbonation efficiency of Ca and Fe was calculated using Equations (5) and (6).

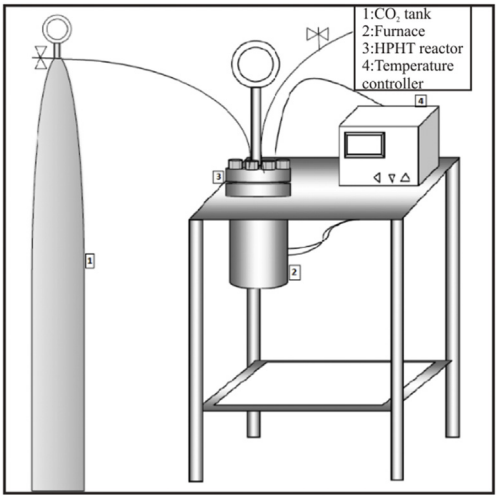

Fig. 1. Schematic diagram of HPHT autoclave reactor.

$$P_{CaCO_3} = \frac{\Delta W(\%) \times Mw_{CaCO_3}}{Mw_{CO_2}} \times 100 \quad (1)$$

$$P_{FeCO_3} = \frac{\Delta W(\%) \times Mw_{FeCO_3}}{Mw_{CO_2}} \times 100 \quad (2)$$

$$\text{Ca mass in } CaCO_3 = \Delta W(\%) \times \frac{Mw_{Ca}}{Mw_{CO_2}} \times \text{mass of solid residue} \quad (3)$$

$$\text{Fe mass in } FeCO_3 = \Delta W(\%) \times \frac{Mw_{Fe}}{Mw_{CO_2}} \times \text{mass of solid residue} \quad (4)$$

$$\text{Ca Carbonation efficiency}(\%) = \frac{\text{Ca mass in } CaCO_3}{\text{Ca total in feeding material}} \times 100 \quad (5)$$

$$\text{Fe Carbonation efficiency}(\%) = \frac{\text{Fe mass in } FeCO_3}{\text{Fe total in feeding material}} \times 100 \quad (6)$$

3. Results and discussion

3.1. XRD analysis of red gypsum

The XRD analysis of red gypsum showed that the red gypsum is mainly composed of gypsum mineral ($CaSO_4 \cdot 2H_2O$). It shows four major peaks at 11.68°, 20.79°, 23.44°, and 29.16°, and some minor peaks at 35.41°, 40.64°, 47.84°, 50.34°, and 51.18° which are assigned to $CaSO_4 \cdot 2H_2O$ in red gypsum as shown in Fig. 2. In addition, the absence of Fe_2O_3 peaks as the other major constituents present in red gypsum could be attributed due to the possibility that the iron can be in amorphous hydroxides because of the high concentration of Fe_2O_3 obtained by XRF [18,23,24].

3.2. XRF analysis of red gypsum

The major and minor constituents of red gypsum were detected using XRF analysis. Fig. 3 shows the EDS spectrum of red gypsum. As shown in this figure, three major peaks were detected and identified as Ca, Fe and S, indicating that these are the major elements of red gypsum. Table 1 also presents the main components of the red gypsum identified from XRF analysis. It can be observed that the red gypsum is mainly composed of CaO (32.2%), Fe_2O_3 (28.99%) and SO_3 (31.6%) together with some insignificant impurities, such as MnO, TiO_2, SiO_2, etc. The compound concentrations are in good agreement with the EDS spectrum of red gypsum, which indicates the presence of Ca, Fe and S as the major constituents of red gypsum.

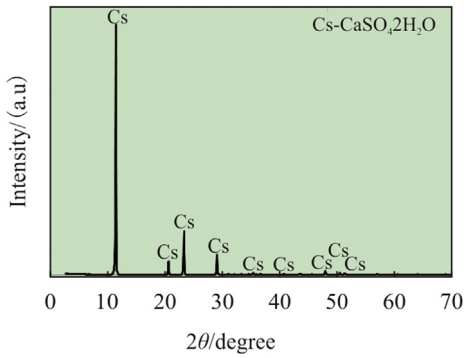

Fig. 2. X-ray diffraction of bulk Red Gypsum.

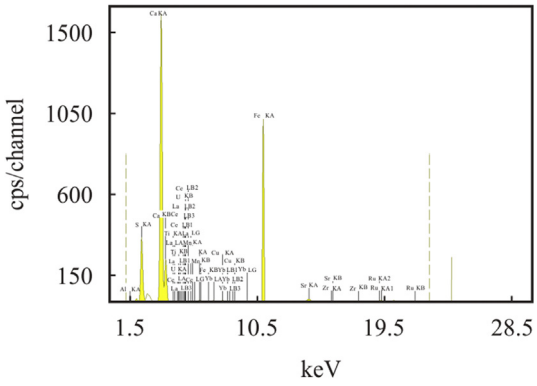

Fig. 3. EDS spectrum of red gypsum.

3.3. ICP-OES analysis of red gypsum

Red gypsum was analyzed with inductively coupled plasma optical emission spectrometry (ICP-OES) to give more exact evidence for the concentrations of different elements in red gypsum. The ICP-OES analysis also showed similar results as XRF in that red gypsum was found to be mainly composed of certain major elements, such as Ca, Fe and S, and also some minor elements in low concentrations, such as Si, Ti, etc., as summarized in Table 2. The concentrations of Ca, Fe and S as the main elements present in red gypsum are 0.23 mg/g, 0.10 mg/g, and 0.12 mg/g, respectively. Some other elements, such as Al, Si, Mn, and Ti, are also present in low concentrations. The concentration of other elements is below 0.001 mg/g, which are not included in this table. As was shown previously, the EDS spectrum results also showed that Ca, Fe, and S are the major elements present in red gypsum. These results are in good agreement with the ICP-OES results, proving that Ca, S, and Fe are the main constituents of red gypsum, which makes it a very potential feedstock for mineral carbonation.

3.4. FT-IR analysis of red gypsum

The chemical structure of red gypsum was analyzed by using a FT-IR spectrophotometer. The samples were prepared as thin films by dilution with KBr and then analyzed using the wavenumber range of 500–4000 cm^{-1}, as shown in Fig. 4. The band centered at 3393 cm^{-1} is due to the stretching vibration of O–H in water molecules. The vibration at 1618 cm^{-1} is also due to the bending of H–*O*–H in water molecules. The presence of the sulphate phase in red gypsum is confirmed by peaks at 1103 and 666 cm^{-1}, and the peak at 1459 is assigned to CO_3^{-2}. The peak at 596 cm^{-1} is the characteristic absorption band of Fe–O in Fe_2O_3. The representative peaks of red gypsum related to four main bonding structures of sulphate, water, carbonate and Fe oxide are in good agreement with the published data in the literature [25,26].

Table 1
Chemical content of red gypsum from XRF.

Compound	Concentration (wt%)
CaO	32.20
SO_3	31.60
Fe_2O_3	28.99
TiO_2	5.64
SiO_2	1.90
Al_2O_3	0.39
MnO	0.41
RuO_2	0.39
Eu_2O_3	0.26
V_2O_5	0.22
ZrO_2	0.06
CuO	0.06
HgO	0.03
Cr_2O_3	0.03
ZnO	0.04
SrO	0.03

3.5. Particle size distribution of red gypsum

Particle size distribution was measured using MASTERSIZER 2000. Two samples of red gypsum were analyzed, and the results are shown in Fig. 5. It is found that the particle size of the red gypsum is in the range of 0.02–2000 μm, with a mean (d_{50}) particle size of 56.03 μm and a specific surface area of 7.01 m^2/g. These values are very close to the reported data in the literature [27]. Particle size analysis for both samples shows that the provided red gypsum is homogeneous, as both samples have similar particle size distributions.

3.6. TGA of red gypsum

Fig. 6 shows the weight-loss and derivative weight-loss behavior of red gypsum as a function of temperature in a nitrogen environment. Initially, 20 mg of red gypsum was used, and 16.98 mg was left over after the experiment. A simple calculation shows that 15.1% of the weight of the red gypsum was reduced by evaporation of some volatile component, including moisture, in the temperature range, while 84.9% of the weight remained in its original solid form. In general, dehydration of gypsum takes place at a temperature range between 80 °C and 250 °C, depending on the heating rate and the composition of the gypsum [28]. The TGA and differential thermal analysis (DTA) curves of red gypsum show that dehydration occurred at temperatures approximately 100–160 °C. The major DTA peak at 137 °C indicated that, during heating of the red gypsum from ambient temperature to 1000 °C, the moisture evaporation rate, including bound and unbound moistures, was the highest at 137 °C. Another weight loss occurs between the temperatures of 600–1000 °C, where the major peak takes place at 709 °C. It is most likely that the weight loss at this range of temperature is due to evaporation of sulphate phases. The evaporation of SO_4 occurs at temperature above 550 °C, SO_3 between 700 and 900 °C and SO_2 between 800 and 1000 °C [29,30].

3.7. FESEM analysis of red gypsum

FESEM analysis was used to elucidate the microstructure and

Table 2
Elemental analysis of red gypsum using ICP-OES.

Element	Concentration (mg/g)
Ca	0.230
S	0.127
Fe	0.101
Ti	0.020
Si	0.009
Mn	0.003
Al	0.002
Ru	0.003
Eu	0.001
Cu	0.001

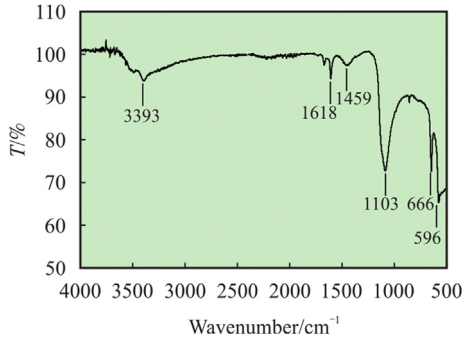

Fig. 4. FT-IR of red gypsum.

morphology of red gypsum. FESEM results show that red gypsum has tubular and prismatic crystal in its structure, which are coated with either thick or thin Fe oxide layers. These coatings might have an effect on the rate of dissolution of red gypsum [23]. According to Lee et al. [31] calcium ions in red gypsum can be easily transformed into calcite and vaterite. Thus, red gypsum can be considered as a very potential and favorable feedstock for mineral carbon dioxide sequestration. Fig. 7 (a) shows some lathlike crystals of gypsum with coatings of Fe oxides, while Fig. 7 (b) shows the fibrous crystal aggregates. Fig. 7 (c) shows that some of the gypsum crystals are thickly coated by the Fe oxides, and Fig. 7 (d) represents the EDS spectrum of red gypsum recorded by FESEM, which proves the existence of Ca and Fe in red gypsum.

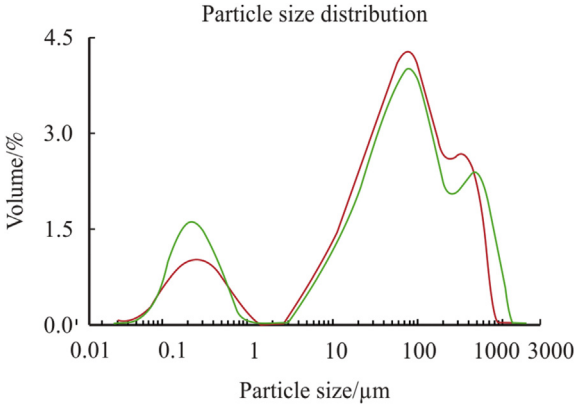

Fig. 5. Particle size distribution for the two bulk red gypsum sample used.

3.8. Carbonation of red gypsum with variable CO_2 pressure

After initial physico-chemical characterization of red gypsum, the effect of CO_2 pressure on direct aqueous carbonation of red gypsum was investigated. Samples of red gypsum with average particle size of less than 45 μm were subjected to carbonation experiments at variable CO_2 pressure (1–70 bar) and constant ambient temperature. The characteristics of final products were analyzed using XRD and TGA.

Fig. 8 represents the Ca/Fe carbonation efficiency and carbonates purity. As shown in this figure, increasing CO_2 pressure has direct effect on carbonation efficiency and products purity. The TGA results showed that under 1 bar CO_2 pressure, only calcium reacted with CO_2 and iron did not react with CO_2, which resulted in zero iron carbonation efficiency and 0.94% calcium carbonation efficiency. However, increasing CO_2 pressure found to be very useful in improving the overall Ca/Fe carbonation efficiency. Under 70 bar CO_2 pressure, the calcium carbonation efficiency and iron carbonation efficiency of 23.59% and 14.28% were achieved, respectively. On the other hand, the $CaCO_3$ and $FeCO_3$ purity also exhibited similar trend as carbonation efficiency. The maximum purity of $CaCO_3$ and $FeCO_3$ in the final products were 14.28% and 5.01%, respectively when CO_2 pressure of 70 bar was used.

The TGA results were supported by performing XRD analysis for two samples. The product samples with 1 bar and 40 bar CO_2 pressure were analyzed with XRD, as shown in Fig. 9. In Fig. 9, spectrum (a) represents the XRD of red gypsum, spectrum (b) for pure $CaCO_3$, spectrum (c) for pure $FeCO_3$, spectrum (d) for the carbonation product with 40 bar CO_2 pressure and spectrum (e) for the carbonation product with 1 bar CO_2 pressure. The TGA results showed that the carbonation experiment with the 1 bar CO_2 pressure results in no $FeCO_3$ formation, which is clearly shown in Fig. 9 as well. The final product's peaks are matched with $CaCO_3$ and red gypsum peaks, without any $FeCO_3$ peaks. However, the other experiment with the 40 bar CO_2 pressure resulted in both $CaCO_3$ and $FeCO_3$ production. Fig. 9 shows the product peaks, which are matched with $CaCO_3$, $FeCO_3$ and red gypsum peaks. In spectrum (d), the peaks at 11.68°, 23.44° and 29.16° are assigned to red gypsum peaks in the final product. The peak at 23.01° is assigned to vaterite, while peaks at 35.88°, 39.33°, 47.42°, 56.48°, and 57.35° are assigned to calcite. The major peak of siderite is observed at 18.54°, which confirms the presence of $FeCO_3$ in the final product. In spectrum (e), the major peaks of red gypsum are observed at 11.68°, 23.44° and 29.16°. The representative peaks at 23.01°, 35.88°, 32.78°, and 47.42 are assigned to vaterite. The representative peaks of calcite are detected at 35.88°, 39.33°, 56.48°, and 57.35°. The detected peaks of calcite, vaterite, siderite and $CaSO_4$ are in good agreement with published data in the literature

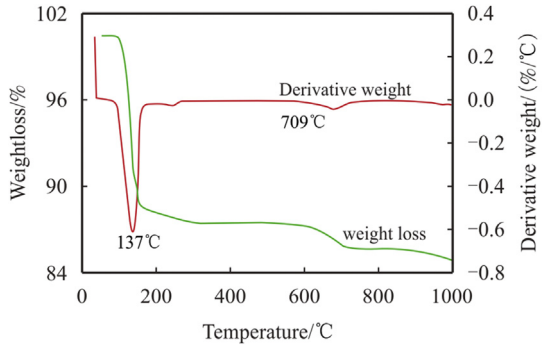

Fig. 6. Weight loss of red gypsum by TGA.

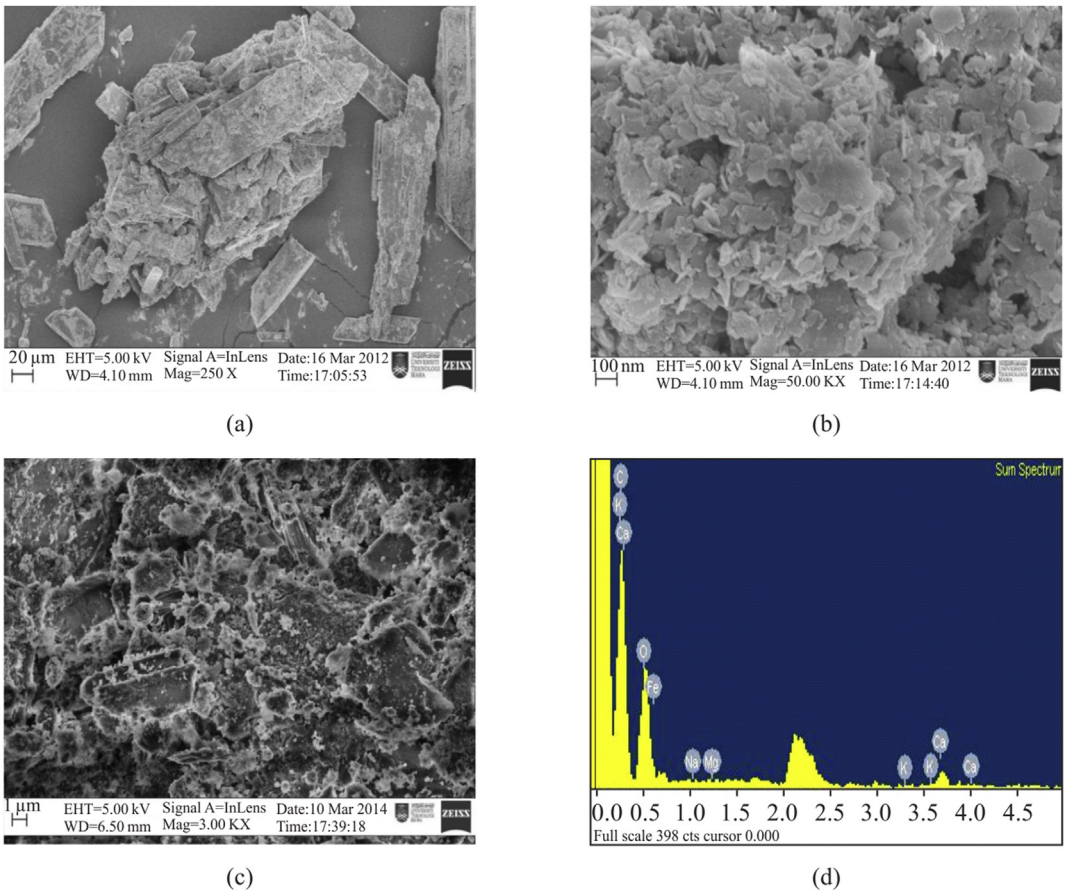

Fig. 7. FESEM and EDX spectra of red gypsum.

[18,32,33].

One of the main reasons for not producing a high purity product in these experiments is because no significant amount of Ca and Fe is extracted from red gypsum to be in reaction with the gaseous CO_2. The favorable condition for the extraction of Ca/Fe ions from red gypsum is lower pH conditions; however, the addition of Nanopure-demineralized water would not lower the solution pH, which is not favorable for metal ion extraction [31,34]. Therefore, low calcium and iron extraction rate from red gypsum seems to be the major obstacle in direct carbonation of red gypsum. On the other hand, increasing CO_2 pressure was found to have positive impact on carbonation efficiency and products purity.

Carbonate precipitation during aqueous mineral carbonation is controlled by the concentration of CO_3^{2-} ions in the solution and also concentration of Ca^{2+}. Mechanistically, increased CO_2 pressure results in greater CO_2 solubility due to the formation and dissociation of carbonic acid. Carbonic acid dissociates, and the equilibrium concentrations of bicarbonate and carbonate are determined by the first and second dissociation constant according to the Henry's law. Because K_{a1}, K_{a2}, and K_H are all constants at a certain temperature, the concentration of CO_3^{2-} will change only as the atmospheric CO_2 partial pressure or pH changes. Therefore, it is feasible to increase the CO_3^{2-} concentration by enhancing the atmospheric CO_2 partial pressure. This explains why increased pressure is not detrimental to carbonation conversion [35]. Wang et al. [36] stated that carbonation efficiency can be improved by increasing either the Ca^{2+} or CO_3^{2-} concentration. At a certain

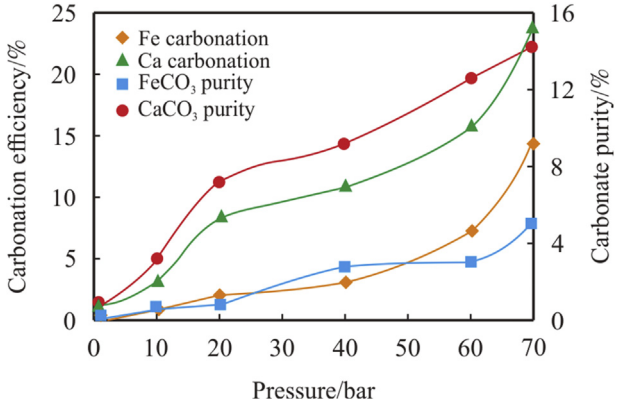

Fig. 8. Carbonation efficiency and products purity with variable CO_2 pressure.

constant temperature, the concentration of CO_3^{2-} will change only as the atmospheric CO_2 partial pressure or pH changes. Therefore, it is feasible to increase the CO_3^{2-} concentration by increasing the CO_2 partial pressure or by increasing the solution pH. This statement is in good agreement with resulted data in the present study in which carbonation efficiency was improved significantly by increasing CO_2 pressure [8,37].

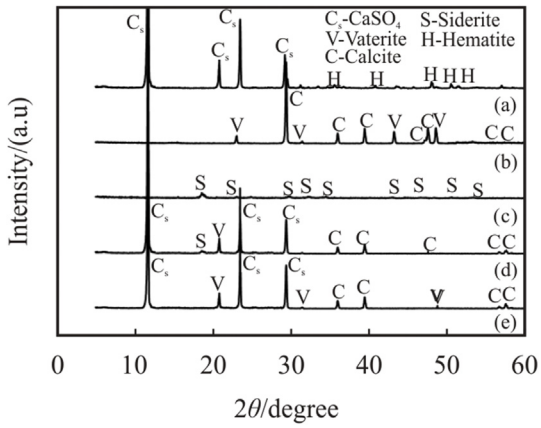

Fig. 9. XRD patterns of (a) Red gypsum; (b) pure $CaCO_3$ (c) pure $FeCO_3$; (d) carbonation at 40 bar; (e) carbonation at 1 bar.

3.9. Carbonation of red gypsum with variable reaction temperature

The effect of reaction temperature on carbonation efficiency and products purity was investigated by applying variable reaction temperature (25–400 °C) at 20 bar CO_2 pressure where red gypsum with particle size of less than 45 μm were utilized.

Fig. 10 presents the Ca/Fe carbonation efficiency and products purity with respect to variabel reaction temperatures. As shown in this figure, Ca/Fe carbonation efficiency is at its minimum value under 25 °C reaction temperature. Further increasing the reaction temperature to about 200 °C results in the maximum Ca/Fe carbonation efficiency, however further increasing the reaction temperature to about 400 °C reduces the overall Ca/Fe carbonation efficiency. The experimental results showed that, the minimum and maximum Ca carbonation efficiency are 6.37% and 12.53%, respectively, while these values are 1.53% and 5.76%, respectively. On the other hand, temperature impact on $CaCO_3$ purity and $FeCO_3$ purity was also the same as carbonation efficiency. The minimum $CaCO_3$ and $FeCO_3$ purity was achieved at 25 °C (5.53% for $CaCO_3$ and 0.75% for $FeCO_3$), and further increasing the reaction temperature to about 200 °C resulted in the maximum $CaCO_3$ and $FeCO_3$ purity of 9.29% and 2.28%, respectively.

Carbonation efficiency in direct carbonation process is function of both metal extraction rate from feedstock and carbonate precipitation rate. Increasing reaction temperature facilitates the extraction of Ca/Fe from red gypsum, which is the reason for increasing the products purity and carboantion efficiency up to 200 °C. On the other hand, according to the Henry's law, increasing reaction temperature increases K_H, K_{a1}, and K_{a2} and lowers K_{sp}. Higher K_{a1} and K_{a2}, and lower K_{sp} are favorable for carbonate precipitation, however the problem arises from higher K_H, which has opposite impact on precipitation rate [18,37,38]. As described by Huijgen et al. [37] and O'Connor et al. [39,40], there are always some optimum temperature in any direct aqueous carbonation process which results in maximum carbonation efficiency. The optimum carbonation rate of steelmaking slag and natural olivine has been found to be 175 °C and 185 °C, respectively.

As stated by Azdarpour et al. [21], setting the reaction temperature below 80 °C results in precipitation of vaterite, aragonite, and calcite. Increasing the reaction temperature to roughly 170 °C favors the precipitation of only vaterite and calcite, and, at temperatures above 170 °C, only vaterite precipitates. Although different morphologies have been reported for different polymorphs of $CaCO_3$, the most common structures of calcite, aragonite and vaterite are rhomboidal, needle/rod and spherical, respectively. Fig. 11 represents the SEM analysis of carbonation product at 200 °C. As shown in this figure, vaterite is produced during the reaction of CO_2 with red gypsum. The purity results showed that $CaCO_3$ with low purity was produced in this process, thus, some fraction of the red gypsum remained unreacted during the process. The unreacted fraction of the red gypsum is also shown in SEM analysis.

3.10. Carbonation of red gypsum with variable particle size

The effect of red gypsum particle size on carbonation efficiency and carbonates purity was investigated by using red gypsum with different particle size of less than 45, 45–100, 100–212, 212–300, and 300–500 μm. The CO_2 pressure of 20 bar at constant reaction temperature of 200 °C were applied. In addition, the reaction time of 60 min was given to each experiments, then the experiments stopped and final products were analyzed accordingly after complete drying in oven. Table 3 represents the calcium and iron carbonation efficiency as well as the carbonates purity with variable particle size of red gypsum.

The carbonation results showed that particle size reduction is very favorable in increasing both carbonation efficiency and carbonates purity. The best result was achieved when red gypsum with average particle size of less than 45 μm was used while increasing the particle size to the highest range of 300–500 μm resulted in the lowest efficiency and carbonates purity. The Fe carbonation efficiency, Ca carbonation efficiency, $FeCO_3$ purity, and

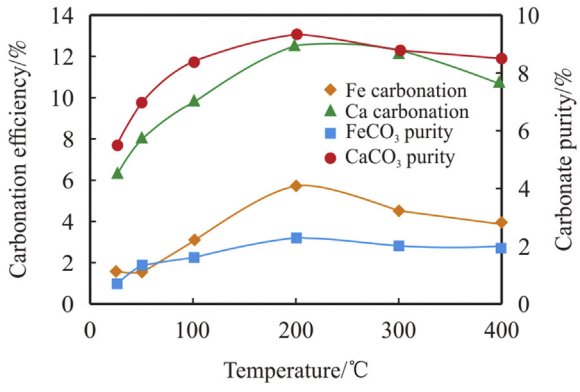

Fig. 10. Carbonation efficiency and products purity with variable reaction temperature.

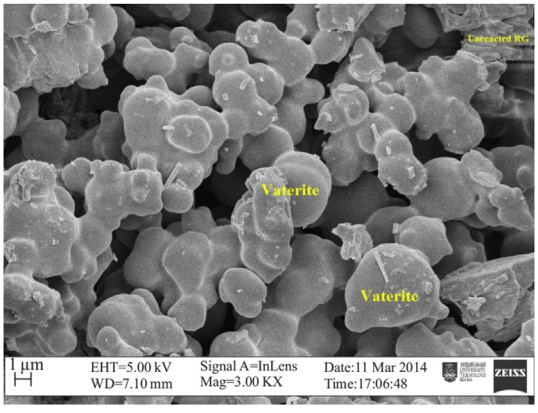

Fig. 11. SEM analysis of carbonate product at 200 °C.

Table 3
Calcium and iron carbonation efficiency and carbonates purity with variable particle size.

Particle size (μm)	Fe Carbonation efficiency (%)	Ca Carbonation efficiency (%)	$FeCO_3$ purity (%)	$CaCO_3$ Purity (%)
<45	5.76	12.53	2.28	9.29
45–100	5.12	11.46	2.01	8.37
100–212	4.74	11.01	1.48	7.11
212–300	4.02	9.37	0.84	5.32
300–500	3.56	8.04	0	4.28

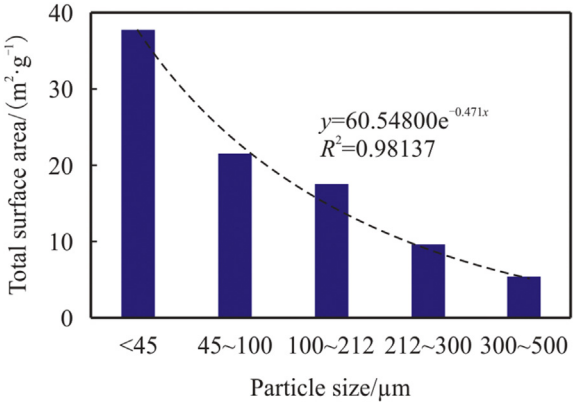

Fig. 12. Total surface area versus different particle size after carbonation experiments using BET analysis.

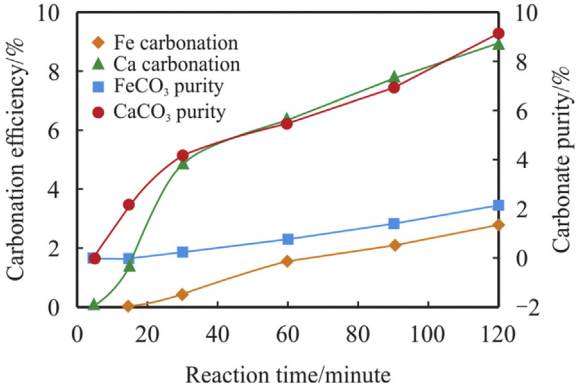

Fig. 14. Carbonation efficiency and carbonates purity with variable reaction time.

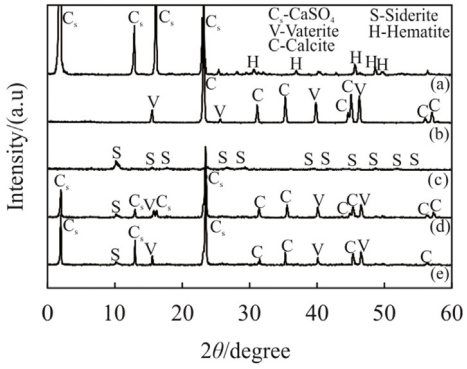

Fig. 13. XRD patterns of (a) red gypsum; (b) pure $CaCO_3$; (c) pure $FeCO_3$; (d) carbonation product of 100–212 μm; (e) carbonation product of 300–500 μm.

$CaCO_3$ purity of 5.76%, 12.53%, 2.28%, and 9.29% were achieved respectively when samples with average particle size of less than 45 μm were used. On the other hand, the values reduced to 3.56%, 8.4%, 0%, and 4.28% for Fe carbonation efficiency, Ca carbonation efficiency, $FeCO_3$ purity, and $CaCO_3$ purity respectively when particles with average size of 300–500 μm were utilized.

As stated by Azdarpour et al. [18], the overall conversion rate of calcium and iron into carbonate is a function of total specific surface area of particles. In addition, particle size reduction increases the total surface area. Therefore, carbonation rate and carbonates purity is increased by decreasing the average particle size of red gypsum. Fig. 12 represents the total surface area of samples after carbonation experiments. This figure clearly indicates that the total surface area increases with decreasing particle size, which results in higher carbonation efficiency and carbonates purity.

Fig. 13 shows the XRD pattern of the carbonated product of red gypsum with 100–212 and 300–500 μm particle sizes. In the XRD pattern, the presence of CaCO3 and FeCO3 peaks confirms the carbonation reaction of Ca and Fe ions with CO2. In Fig. 13, the spectra (a), (b), (c), (d), and (e) represent the red gypsum, pure CaCO3, pure FeCO3 and reaction product of 100–212 and 400–500 μm particle sizes, respectively. The spectrums (d) and (e) represent the XRD pattern of the carbonation product of red gypsum. In these spectrums, the significant representative peaks of calcite and vaterite as mentioned above are present, implying that the CaCO3 is successfully formed in the carbonation reaction. Although the peak intensity of FeCO3 in spectrum (c) is low, it is also present in the product spectrums (d and e). In addition, the representative peaks of Ca sulphate are also present, which implies that some fraction of red gypsum (most likely a significant fraction) remained unreacted during the direct carbonation. The peak intensities of calcite and vaterite in spectrum (d) are higher than in spectrum (e), which is due to the higher purity of carbonate products. However, the peak intensities of Ca sulphate are higher in spectrum (e) than spectrum (d), which shows that the purity of red gypsum is higher in spectrum (e) compared to spectrum (d).

3.11. Carbonation of red gypsum with variable reaction time

The carbonation time of 5–120 min were applied to investigate the effects of reaction time on carbonation efficiency and carbonates purity. In these experiments, the CO_2 pressure of 20 bar, reaction temperature of 25 °C, and red gypsum with average particle size of less than 45 μm were utilized constantly. Fig. 14 represents the carbonation efficiency and carbonates purity with respect to different reaction time.

The experimental results showed that carbonation efficiency and carbonates purity are in direct relationship with reaction time in which increasing the reaction time increased efficiency and purity. Initially, the carbonation experiments were given 5 min,

which resulted in 0% Fe and Ca carbonation efficiency. This shows that after 5 min of reaction time, no reaction took place between red gypsum and CO_2. However, after increasing the reaction time to about 30 min, the Fe and Ca carbonation efficiency increased to 0.45% and 4.83%, respectively. At this time, the purity of $FeCO_3$ and $CaCO_3$ was about 0.25% and 4.13%, respectively. Finally, by increasing the reaction time to 120 min, the maximum Fe and Ca carbonation efficiency of 2.85% and 8.94% were achieved, respectively. Meanwhile, the maximum purity of $FeCO_3$ and $CaCO_3$ were 2.11% and 9.12%, respectively.

The results of these experiments are in good agreement with the results of Huijgen et al. [37,38]. They investigated the effects of retention time by changing the retention times from 2 to 30 min during direct carbonation of steel slag. Their results showed that the maximum achieved conversion rate was at 30 min compared to the minimum conversion rate at 2 min. They finally concluded that a longer reaction time increases the conversion rate of Ca into its carbonate form. Katsuyama et al. [41] also concluded that increasing the retention time produces higher purity $CaCO_3$ from waste cement. From the literature data, it is very clear that increasing retention time has a positive effect on product purity and overall carbonation efficiency. The reason behind this phenomenon is that, by increasing the reaction time, the reactants (Ca and Fe ions) have more time to react with the gaseous CO_2. Therefore, higher purity products and higher carbonation efficiency are achieved by increasing the reaction time.

4. Conclusions

The physical and chemical characteristics of red gypsum were investigated using major instrumental analysis such as XRD, XRF, SEM, ICP-OES, FT-IR, TGA and MASTERSIZER2000. The XRD result showed that red gypsum mainly consists of $CaSO_4 \cdot 2H_2O$. This result was further supported by XRF, SEM and ICP-OES results which proved that calcium and iron are the major constituents of red gypsum which makes it a very suitable and potential feedstock for mineral carbonation. Furthermore, the FT-IR spectra proved the presence of sulphate and iron bonds in red gypsum. In addition, particle size analysis showed that the average particle size of red gypsum is 0.02–2000 μm with the mean (d_{50}) particle size of 56.03 μm and the specific surface area of 7.01 m^2/g. Moreover, the carbonation results showed that both $CaCO_3$ and $FeCO_3$ could be produced during direct aqueous carboantion of red gypsum with Nanopure-distilled water, however, the process needs to be further optimized to achieve higher carbonation rates alongside high purity products.

Acknowledgments

The authors would like to appreciate the Department of Petroleum Engineering, Marvdasht Branch, Islamic Azad University, Marvdasht, Iran for the provision of the laboratory facilities necessary for completing this work.

References

[1] E.R. Bobicki, Q. Liu, Z. Xu, H. Zeng, Carbon capture and storage using alkaline industrial wastes, Prog. Energy Combust. Sci. 38 (2012) 302–320.
[2] G. Li, Numerical investigation of CO_2 storage in hydrocarbon field using a geomechanical-fluid coupling model, Petroleum 2 (2016) 252–257.
[3] M.A. Ahmadi, M. Zeinali Hasanvand, S. Shokrolahzadeh, Technical and economic feasibility study of flue gas injection in an Iranian oil field, Petroleum 1 (2015) 217–222.
[4] I.M. Kang, K.M. Roh, Mineral carbonation of gaseous carbon dioxide using a clay-hosted cation exchange reaction, Int. J. Min. Reclam. Environ. 34 (2013) 3191–3195.
[5] S. Jung, G. Dodbida, T. Fujita, Mineral carbonation by blowing incineration gas containing CO_2 into the solution of fly ash and ammonia for ex situ carbon capture and storage, Int. J. Min. Reclam. Environ. 17 (2014) 125–135.
[6] M.Y. Lee, K.W. Ryu, S.C. Chae, Y.N. Jang, Effects of temperature on the carbonation of flue gas desulphurization gypsum using a CO_2/N_2 gas mixture, Int. J. Min. Reclam. Environ. 36 (2015) 106–114.
[7] A.A. Olajire, A review of mineral carbonation technology in sequestration of CO_2, J. Petrol. Sci. Eng. 109 (2013) 364–392.
[8] R.M. Santos, J. Van Bouwel, E. Vandevelde, G. Mertens, J. Elsen, T. Van Gerven, Accelerated mineral carbonation of stainless steel slags for CO_2 storage and waste valorization: effect of process parameters on geochemical properties, Int. J. Greenh. Gas Control 17 (2013) 32–45.
[9] R.M. Santos, M. Bodor, P.N. Dragomir, A.G. Vraciu, M. Vlad, T. Van Gerven, Magnesium chloride as a leaching and aragonite-promoting self-regenerative additive for the mineral carbonation of calcium-rich materials, Miner. Eng. 59 (2014) 71–81.
[10] R.M. Santos, Y.W. Chiang, J. Elsen, T. Van Gerven, Distinguishing between carbonate and non-carbonate precipitates from the carbonation of calcium-containing organic acid leachates, Hydrometallurgy 147–148 (2014) 90–94.
[11] A. Azdarpour, M. Asadullah, R. Junin, M. Manan, H. Hamidi, A.R.M. Daud, Carbon dioxide mineral carbonation through pH-swing process: a review, Energy Procedia 61 (2014) 2783–2786.
[12] A. Azdarpour, M. Asadullah, H. Hamidi, M. Manan, A.R.M. Daud, Calcium carbonate production through direct mineral carbon dioxide sequestration, Appl. Mech. Mater 699 (2015) 1020–1025.
[13] A. Azdarpour, M. Asadullah, E. Mohammadian, H. Hamidi, R. Junin, M. Afkhami Karaei, A review on carbon dioxide mineral carbonation through pH-swing process, Chem. Eng. J. 279 (2015) 425–436.
[14] m. Dri, A. Sanna, M.M. Maroto-Valer, Dissolution of steel slag and recycled concrete aggregate in ammonium bisulphate for CO_2 mineral carbonation, Fuel Process. Technol. 113 (2013) 114–122.
[15] A. Sanna, X. Wang, A. Lacinska, M. Styles, T. Paulson, M.M. Maroto-Valer, Enhancing Mg extraction from lizardite-rich serpentine for CO_2 mineral sequestration, Min. Eng. 49 (2013) 135–144.
[16] A. Sanna, M. Dri, M.M. Maroto-Valer, Carbon dioxide capture and storage by pH swing aqueous mineralisation using a mixture of ammonium salts and antigorite source, Fuel 114 (2013) 153–161.
[17] A. Sanna, A. Lacinska, M. Styles, M.M. Maroto-Valer, Silicate rock dissolution by ammonium bisulphate for pH swing mineral CO_2 sequestration, Fuel Process. Technol. 120 (2014) 128–135.
[18] A. Azdarpour, M. Asadullah, R. Junin, M. Manan, H. Hamidi, E. Mohammadian, Direct carbonation of red gypsum to produce solid carbonates, Fuel Process. Technol. 126 (2014) 429–434.
[19] A. Azdarpour, M. Asadullah, R. Junin, E. Mohammadian, H. Hamidi, A.R.M. Daud, M. Manan, Extraction of calcium from red gypsum for calcium carbonate production, Fuel Process. Technol. 130 (2015) 12–19.
[20] S.M. Pérez-Moreno, M.J. Gázquez, J.P. Bolívar, CO_2 sequestration by indirect carbonation of artificial gypsum generated in the manufacture of titanium dioxide pigments, Chem. Eng. J. 262 (2015) 737–746.
[21] A. Azdarpour, M. Asadullah, E. Mohammadian, R. Junin, H. Hamidi, M. Manan, A.R.M. Daud, Mineral carbonation of red gypsum via pH-swing process: effect of CO_2 pressure on the efficiency and products characteristics, Chem. Eng. J. 264 (2015) 425–436.
[22] M.J. Gázquez, J.P. Bolívar, R. García-Tenorio, F. Vaca, Physicochemical characterization of raw materials and co-products from the titanium dioxide industry, J. Hazard. Mater. 166 (2009) 1429–1440.
[23] I. Fauziah, S. Zauyah, T. Jamal, Characterization and land application of red gypsum: a waste product from the titanium dioxide industry, Sci. Total Environ. 188 (1996) 243–251.
[24] A. Telesca, M. Marroccoli, D. Calabrese, G.L. Valenti, F. Montagnaro, Flue gas desulfurization gypsum and coal fly ash as basic components of prefabricated building materials, Waste Manag. 33 (2013) 628–633.
[25] A. Karaipekli, A. Sarı, Preparation and characterization of fatty acid ester/building material composites for thermal energy storage in buildings, Energy Build. 43 (2011) 1952–1959.
[26] C. Paluszkiewicz, J. Czechowska, A. Ślósarczyk, Z. Paszkiewicz, Evaluation of a setting reaction pathway in the novel composite TiHA-CSD bone cement by FT-Raman and FT-IR spectroscopy, J. Mol. Struct. 1034 (2013) 289–295.
[27] Y.S. Park, H.N. Shin, D.H. Lee, D.J. Kim, J.H. Kim, Y.K. Lee, S.J. Sim, K.B. Choi, Drying characteristics of particles using thermogravimetric analyzer, Korean J. Chem. Eng. 20 (2003) 1170–1175.
[28] I.Y. Elbeyli, S. Piskin, Thermal dehydration kinetics of gypsum and borogypsum under Non-isothermal conditions, Chin. J. Chem. Eng. 12 (2004) 302–305.
[29] J. Majzlan, C. Botez, P.W. Stephens, The crystal structures of synthetics $Fe_2(SO_4)_3(H_2O)_5$ and the type specimen of lausenite, Am. Mineral. 90 (2005) 411–416.
[30] P.D. Sahare, J.S. Bakare, S.D. Dhole, P. Kumar, Effect of phase transition and particle size on thermoluminescence characteristics of nanocrystalline $K_2Ca_2(SO_4)_3$:Cu^+ phosphor, Radiat. Meas. 47 (2012) 1083–1091.
[31] M.G. Lee, Y.N. Jang, K.W. Ryu, W. Kim, J.H. Bang, Mineral carbonation of flue gas desulfurization gypsum for CO_2 sequestration, Energy. 47 (2012) 370–377.
[32] S.K. Sahoo, K. Agarwal, A.K. Singh, B.G. Polke, K.C. Raha, Characterization of γ- and α-Fe_2O_3 nano powders synthesized by emulsion precipitation-calcination route and rheological behaviour of α-Fe_2O_3, Int. J. Eng. Sci. Technol. 2 (2010)

118–126.
[33] Q. Dong, N. Kumada, Y. Yonesaki, T. Takei, N. Kinomura, D. Wang, Template-free hydrothermal synthesis of hollow hematite Microspheres, J. Mater. Sci. 45 (2010) 5685–5691.
[34] J.H. Bang, Y.N. Jang, W. Kim, K.S. Song, C.W. Jeon, S.C. Chae, S.W. Lee, S.J. Park, M.G. Lee, Precipitation of calcium carbonate by carbon dioxide microbubbles, Chem. Eng. J. 174 (2011) 413–420.
[35] N.A. Meyer, J.U. Vogeli, M. Becker, J.L. Broadhurst, D.L. Reid, J.P. Franzidis, Mineral carbonation of PGM mine tailings for CO_2 storage in South Africa: a case study, Miner. Eng. 59 (2014) 45–51.
[36] W. Wang, M. Hu, Y. Zheng, P. Wang, C. Ma, CO_2 fixation in Ca^{2+}-/Mg^{2+}-Rich aqueous solutions through enhanced carbonate precipitation, Ind. Eng. Chem. Res. 50 (2011) 8333–8339.
[37] W.J.J. Huijgen, G.J. Witkamp, R.N.J. Comans, Mineral CO_2 sequestration by steel slag carbonation, Environ. Sci. Technol. 39 (2005) 9676–9682.
[38] W.J.J. Huijgen, G.J. Witkamp, R.N.J. Comans, Mechanisms of aqueous wollastonite carbonation as a possible CO_2 sequestration process, Chem. Eng. Sci. 61 (2006) 4242–4251.
[39] O'Connor, W.K.; Dahlin, D.C.; Nilsen, D.N.; Rush, G.E.; Walters, R.P.; Turner, P.C. CO2 storage in solid form: a study of direct mineral carbonation. In: The 5th international conference on greenhouse gas technologies. 12–15 August, 2000, Cairns, Australia.
[40] W.K. O'Connor, D.C. Dahlin, G.E. Rush, S.J. Gerdemann, L.R. Penner, Energy and economic evaluation of ex situ aqueous mineral carbonation, Greenh. Gas. Control Technol. 7 (2005) 2011–2015.
[41] Y. Katsuyama, A. Yamasaki, A. Iizuka, M. Fujii, K. Kumagai, Y. Yanagisawa, Development of a process for producing high-purity calcium carbonate ($CaCO_3$) from waste cement using pressurized CO_2, Environ. Prog. 24 (2005) 162–170.